

Coumarin-Based Inhibitors of Human NAD(P)H:Quinone Oxidoreductase-1. Identification, Structure–Activity, Off-Target Effects and In Vitro Human Pancreatic Cancer Toxicity

Karen A. Nolan,[†] He Zhao,[‡] Paul F. Faulder,[†] A. David Frenkel,[†] David J. Timson,[§] David Siegel,^{||} David Ross,^{||} Terrence R. Burke Jr.,[‡] Ian J. Stratford,^{*,†} and Richard A. Bryce^{*,†}

School of Pharmacy and Pharmaceutical Sciences, University of Manchester, Oxford Road, Manchester, M13 9PT, U.K., Laboratory of Medicinal Chemistry, National Cancer Institute, National Institutes of Health, Bethesda, Maryland 20892, School of Biological Sciences, Queen's University Belfast, Medical Biology Centre, 97 Lisburn Road, Belfast, BT9 7BL, U.K., and Department of Pharmaceutical Sciences and Cancer Center, School of Pharmacy, University of Colorado and Health Sciences Center, Denver, Colorado 80220

Received April 21, 2007

The enzyme human NAD(P)H quinone oxidoreductase-1 (NQO1), which is overexpressed in several types of tumor cell, is considered a design target for cancer therapeutics. We identify new coumarin-based competitive inhibitors of NQO1, one of which is nanomolar. Using computational docking and molecular dynamics, we obtain insights into the structural basis of inhibition. Selected inhibitors were then assessed for off-target effects associated with dicoumarol and were found to have differing effects on superoxide formation and mitochondrial respiration. A comparison of NQO1 inhibition and off-target effects for dicoumarol and its derivatives suggests that the ability of dicoumarol to kill cancer cells is independent of NQO1 inhibition, that cellular superoxide production by dicoumarol does not seem linked to NQO1 inhibition but may be related to mitochondrial decoupling, and that superoxide does not appear to be a major determinant of cytotoxicity. Implications are discussed for NQO1 inhibition as an anticancer drug design target and superoxide generation as the dicoumarol-mediated mechanism of cytotoxicity.

Introduction

NAD(P)H quinone oxidoreductase-1 (NQO1, DT-diaphorase) was first detected in and isolated from the soluble fraction of rat-liver homogenates.¹ It is a ubiquitous flavoprotein that is widely distributed in animals, plants, and bacteria.² Several properties of NQO1 make it a unique enzyme. These include its ability to use pyridine nucleotides, NADH and NADPH, with equal efficiency,³ its obligatory two-electron reduction of a wide range of substrates,⁴ and its extreme sensitivity to inhibition by the anticoagulant, dicoumarol or 3,3'-methylenebis(4-hydroxycoumarin)⁵ (**1**, Figure 1A). NQO1 is generally considered to be a detoxification enzyme that has been shown to prevent the formation of reactive oxygen species, play an antioxidant role by maintaining ubiquinones, α -tocopherolhydroquinone, and α -tocopherol in their reduced forms,⁶ and regulate intracellular redox state by controlling the NAD(P)H:NAD(P)⁺ ratio.⁷ Human (h)NQO1 has been found to be up-regulated in pancreatic cancer, as well as many other solid tumors. Inhibition of hNQO1 can inhibit growth of pancreatic cancer cells and the underlying mechanism may involve interference with the antioxidant activity of NQO1.⁸ Additional functions of the enzyme include the bioactivation of certain antitumor quinones such as mitomycin C (6-amino-1,1a,2,8,8a,8b-hexahydro-8-(hydroxymethyl)-8a-methoxy-5-methyl-azirino[2',3':3,4]pyrrolo[1,2-a]indole-4,7-dione carbamate), EO9 (3-hydroxy-5-aziridinyl-1-methyl-2-(1H-indole-4,7-dione)-prop- β -en- α -ol), RH1 (2,5-diaziridinyl-3-(hydroxymethyl)-6-methyl-1,4-benzoquinone), streptonigrin (5'-amino-6'-(7-amino-5,8-dihydro-6-methoxy-5,8-

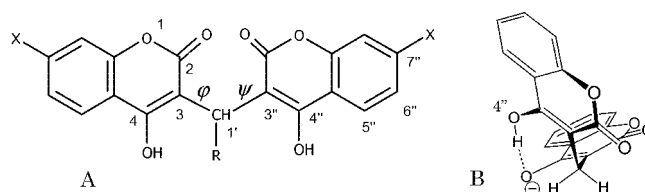


Figure 1. (A) Chemical structure and numbering scheme of dicoumarol **1** (R = H, X = H) and analogues; linker torsion angles φ and ψ are defined in the text. The numbering convention applied is such that the left-hand coumarin ring is the one that π -stacks with FAD. (B) Modeled monoanionic tautomer of **1**.

dioxo-2-quinolyl)-4'-(8'-hydroxy-9'-methoxyphenyl)3'-methyl-2'-pyridinecarboxylic acid), and β -lapachone (3,4-dihydro-2,2-dimethyl-2H-naphtho(1,2-b)pyran-5,6-dione); these observations have led to NQO1 being considered a target for rational anticancer drug design.⁹ More recently, studies have shown that NQO1 plays an important part in regulating the stability of the tumor suppressor protein p53 and several other short-lived proteins including p73 α and ornithine decarboxylase.^{10a}

Structural studies have shown that hNQO1 exists as a homodimer with 274 residues per monomer, each with a molecular mass of 30 867 Da.⁴ Each subunit contains one molecule of flavin adenine dinucleotide (FAD) which is noncovalently attached to the protein. FAD is orientated such that its isoalloxazine ring forms the floor of the NQO1 active site cavity.^{4,11} Two active sites are positioned at opposite ends of the dimer and contain residues from both monomers.^{4,11} The catalytic cycle of NQO1 functions via a "ping-pong" mechanism that is proposed to occur in two distinct steps: hydride transfer from NAD(P)H to the FAD cofactor, followed by release of NAD(P)⁺ and hydride transfer from the reduced cofactor to the

* To whom correspondence should be addressed. Phone: (+44) (0)161 275 8345 (R.A.B.); (+44) (0)161 275 2487 (I.J.S.). Fax: (+44) (0)161 275 2481 (R.A.B.); (+44) (0)161 275 8342 (I.J.S.). E-mail: Richard.Bryce@manchester.ac.uk (R.A.B.); Ian.Stratford@manchester.ac.uk (I.J.S.).

[†] University of Manchester.

[‡] National Cancer Institute.

[§] Queen's University Belfast.

^{||} University of Colorado and Health Sciences Center.

^aList of abbreviations: human NAD(P)H quinone oxidoreductase-1, hNQO1; molecular dynamics, MD; National Cancer Institute, NCI; bovine serum albumin, BSA.

substrate.^{4,11} Many coumarins, flavones, and Cibacron blue are competitive inhibitors of NQO1.¹² However, dicoumarol (**1**) is thought to be the most potent competitive inhibitor of NQO1 (Figure 1), vying with NAD(P)H for binding to NQO1 and thus preventing electron transfer to FAD.⁵ Dicoumarol is frequently used to study the consequences of a lack of NQO1 function in cells, and many pharmacological studies of NQO1 rely on the use of this inhibitor.¹³ However, there are major drawbacks with the use of dicoumarol in cellular systems: these include its binding to serum albumin¹⁴ and its off-target effects such as increasing oxygen radical formation and inhibiting oxygen respiration.

In this work, we mine the National Cancer Institute (NCI) compound database to identify novel coumarin-based inhibitors of NQO1 and perform docking and molecular dynamics to understand the structural basis of inhibition. We subsequently assess a selected number of these NQO1 inhibitors for superoxide formation, oxygen respiration, and cytotoxicity in MIA PaCa-2 human pancreatic carcinoma cells in vitro. From these studies, we then discuss the implications for inhibition of NQO1 as a target for anticancer drug design and superoxide generation as the mechanism of cytotoxicity mediated by dicoumarol.

Results

Structure–Activity Relationships. From a computational search of the NCI database for chemical compounds possessing the dicoumarol substructure, 54 compounds were identified of the general structure indicated in Figure 1, of which 25 were available for evaluation as described in the Experimental Methods section. This was supplemented by one additional coumarin-based ligand, **24** (Table 1). The ability of these 26 compounds to inhibit recombinant hNQO1 was then evaluated in vitro (Table 1). All compounds were assayed in the presence and absence of bovine serum albumin (BSA), providing information on the effect of nonspecific protein binding, often a particular problem with charged species. The coumarin analogues identified from the NCI possess a diverse range of chemical structures, with considerable variation in size from a single coumarin ring, such as compound **24**, to four coumarin rings, such as **4**, **8**, and **25** (Table 1). Correspondingly, a range in inhibitory potency against hNQO1 is observed. An IC₅₀ value of 5 nM is exhibited (in the absence of BSA) by dicoumarol (**1**) and compound **2**, the 7-hydroxy analogue of dicoumarol (Table 1); this compares with an IC₅₀ value of around 8 μM for the phenyl- and pyridyl-substituted derivatives of **2**, denoted **15** and **17**, respectively (Table 1). We observe that **2** exhibits the greatest inhibition of the 26 compounds both in the absence or presence of BSA (5 nM and 0.35 μM, respectively), and **15** shows approximately the poorest levels of NQO1 inhibition in both cases, 7.5 and 82 μM, respectively (Table 1). A low correlation is found between observed IC₅₀ value in the absence and presence of BSA ($r^2 = 0.34$).

To obtain further insight into the relationship between observed inhibition of these compounds and the structure of their interactions with the active site of hNQO1, computational docking via the genetic-algorithm based program GOLD was used in conjunction with the ChemScore scoring function.^{15,16} Earlier work has shown that ChemScore often outperforms other scoring functions.^{16–18} We have previously performed validation tests for docking into the active site of NQO1 via GOLD using three compounds, RH1, ES936 (5-methoxy-1,2-dimethyl-3-[(4-nitrophenoxy)methyl]indole-4,7-dione), and EO9. The three ligands were docked back into their native complexes using GOLD/ChemScore with a root-mean-square deviation in

atomic position of less than 1.4 Å and recovery of all native hydrogen bonds.¹⁹ Here, we consider the ability of docking calculations to energetically rank the 26 coumarin-based compounds according to their experimentally observed affinity (Table 1). We dock into the very recently available crystal complex of dicoumarol **1** with hNQO1 (PDB code 2F1O, resolution 2.75 Å).²⁰

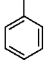
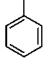
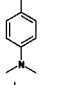
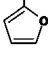
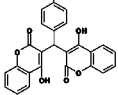
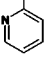
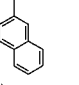
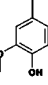
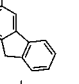
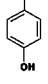
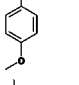
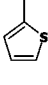
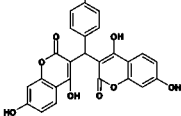
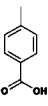
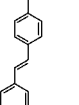
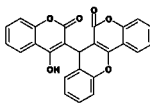
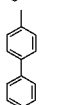
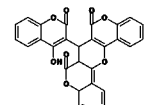
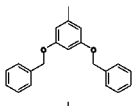
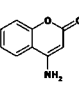
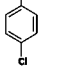
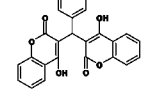
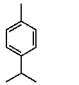
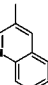
As discussed in the Experimental Methods section, dicoumarol and some of its derivatives in Table 1 may exist as a mixture of dianion and monoanion under assay conditions of pH 7.4. The most favorable monoanionic form of **1**, as indicated from quantum mechanics calculations, is shown in Figure 1B. Docking either the dianionic or monoanionic form of the compound set into NQO1 leads to a correlation between calculated and experimental binding free energy which is not strong ($r^2 < 0.1$, no BSA). However, this correlation includes compounds which appeared too large to dock sufficiently deeply into the active site of NQO1 (**4**, **8**, **23**, and **25**). It also seems that compound **2** is an outlier, with underprediction of its binding affinity by ChemScore by 5.4–5.8 kcal/mol (Table 1). Exclusion of these five compounds gives an improved squared regression coefficient for the ligand set, with a value of 0.52 when dicoumarol-like species were modeled in a dianionic state and 0.53 when modeled in a monoanionic state (Figure 2). This compares with results obtained from GOLD/ChemScore analysis of a set of 60 protein–ligand crystal structures, where a r^2 value of 0.53 with the experimentally observed binding affinities was found.¹⁶ As in our previous study of nondicoumarol NQO1 ligands,¹⁹ we note that correlation did not markedly improve with docking into different crystal structures (PDB codes 1H66, 1GG5, and 1KBQ)^{11,22} nor was there a strong correlation when using an experimental binding affinity from the assay performed in the presence of BSA.

From this relationship (Figure 2), both calculated and experimental affinities clearly indicate that substitution at the linker connecting the two coumarin rings of the dicoumarol motif (R in Figure 1A) significantly reduces inhibitory potency with respect to unsubstituted **1**. The docked conformation of **1** in either dianionic or monoanionic form corresponds closely to the crystallographic pose of **1** (Figure 3), with heavy-atom rmsd values of 0.85 and 0.78 Å, respectively. Thus, the internal geometries of the docked and crystal structures of **1** are similar, forming a bent shape. We define the CH₂ linker torsion angles between the coumarin rings, C2–C3–C1'–C3'' and C3–C1'–C3''–C2'', as φ and ψ , respectively (Figure 1). Calculated φ/ψ values of (73°, –106°) and (78°, –104°) are found for the docked dianion and monoanion poses of **1**, respectively, which compares well to (82°, –97°) in the crystal (Figure 3).

Correspondingly, one coumarin ring of **1** π -stacks with FAD in the NQO1 active site (Figure 4). Specifically, the heterocyclic ring of one of the 4-hydroxycoumarin components of dicoumarol forms a sandwich stack with a terminal ring of the isoalloxazine moiety of FAD (Figure 4). Oxygen O4 of this coumarin ring forms a hydrogen bond with His161 (in the crystal, reassignment of the histidine ring heteroatoms leads to a N ϵ_2 ...O4 distance of 2.83 Å). A hydrogen bond is formed by atoms O1 and O2 of the coumarin ring to O η of Tyr128 of NQO1 (in the crystal, these interatomic distances are 2.79 and 3.31 Å, respectively). The second coumarin ring points away from the FAD, sitting in the active site access channel formed by Tyr128 and His194 (Figure 4).

The docked poses for both monoanionic or dianionic linker-substituted ligands suggest that these compounds, while forming polar contacts, experience steric hindrance, losing their ability

Table 1. Dicoumarol Analogues and Coumarin Derivatives, Values of Experimental IC₅₀ (μ M) for Inhibition of Purified Recombinant hNQO1, and Computed Ligand/NQO1 Binding Free Energy (ΔG_{calc}) Calculated Using ChemScore (kcal/mol)

Compound	R	X	ΔG_{calc}^a	IC ₅₀ ^b	Compound	R	X	ΔG_{calc}^a	IC ₅₀ ^b
1	H	H	-8.7 (-8.0)	0.005 (0.45)	14		H	-5.2 (-5.3)	4.2 (21)
2	H	OH	-6.3 (-5.9)	0.005 (0.35)	15		OH	-3.5 (-3.6)	7.5 (82)
3		H	-6.0 (-6.1)	0.10 (5)	16		H	-5.7 (-4.5)	1.3 (5.9)
4		H	-3.2 (-3.0)	0.11 (20)	17		OH	-3.6 (-4.8)	8 (24)
5		H	-5.7 (-6.5)	0.14 (8.5)	18		H	-5.0 (5.0)	0.65 (10)
6		H	-7.0 (-6.7)	0.15 (41)	19		H	-5.3 (-5.1)	2.3 (35)
7		H	-5.5 (-5.6)	0.22 (8.7)	20		H	-6.7 (-6.4)	0.55 (10)
8		OH	0.4 (-0.9)	0.25 (55)	21		H	-4.9 (-4.8)	1.7 (21)
9		H	-7.0 (-7.1)	0.35 (60)	22 ^c		-	-7.2	0.2 (0.65)
10		H	-6.7 (-6.2)	0.88 (44.5)	23 ^c		-	-2.3	0.25 (0.60)
11		H	-5.9 (-6.6)	1.25 (50)	24 ^c		-	-6.7	3.25 (13)
12		H	-5.9 (-5.3)	2.2 (28)	25		H	-4.9 (-3.1)	0.5 (22.5)
13		H	-6.0 (-6.0)	3.5 (29)	26		H	-6.0 (-6.2)	0.38 (18)

^a Values in parentheses are ChemScore values for docking of ligand in dianion form where applicable. ^b Values of IC₅₀ in parentheses are obtained in the presence of BSA. ^c Structures shown in table are complete molecule, not R group; molecules do not have a dianionic form.

to form a π -stack effectively with the FAD isoalloxazine ring (Figure 4); this was in fact reflected in larger protein–ligand clash contributions to calculated scores relative to nonlinker-substituted compounds **1**, **2**, and **24**. We observe that moderately sized substituents at R typically dock with the coumarin ring stacking against FAD, as for compound **19** (Figure 5A), although other low-lying docking solutions predict the planar R group to lie above FAD. It is also interesting to note that compound **23** has a reasonably good observed affinity (0.25 μ M) but very low predicted affinity (41 mM). This appears to arise in part from large protein–ligand clash terms, which to some extent would be ameliorated by incorporating a level of protein flexibility.

As observed earlier, dicoumarol **1** and analogue **2** are the most potent inhibitors considered in this study (both 5 nM). However, compound **2** is not well accounted for via the computed ChemScore energies of -5.9 kcal/mol for the dianion and -6.3 kcal/mol for the monoanion (Table 1), relative to an experimental value of -11.7 kcal/mol. Compound **2** differs from compound **1** by the presence of two hydroxyl groups at position 7 of the coumarin rings (X in Figure 1A). The decreased docking score for **2** appears to mostly stem from a smaller lipophilic score than **1** (by 1.2 kcal/mol for the monoanion). This may arise from poorer packing against FAD, resulting from the presence of the extra 7-OH groups, coupled to a lack of amino acid side chain flexibility in docking (Figure 5B). The docked

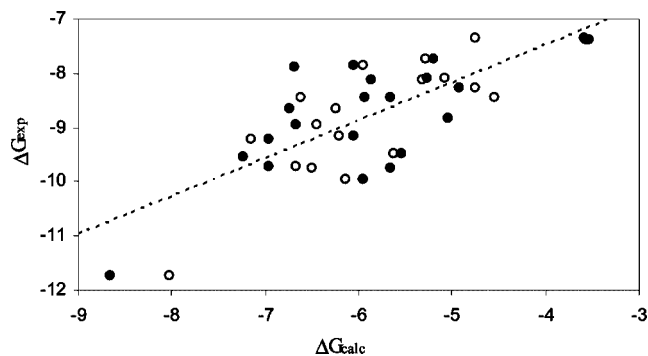


Figure 2. Calculated and experimental binding affinity in the absence of BSA (kcal/mol) for dicoumarol-like species modeled in dianionic (white circles) and monoanionic states (black circles). ΔG_{exp} is calculated as $-RT \ln(1/K_i)$, where K_i is obtained from IC_{50} values using the Cheng–Prusoff equation.²¹

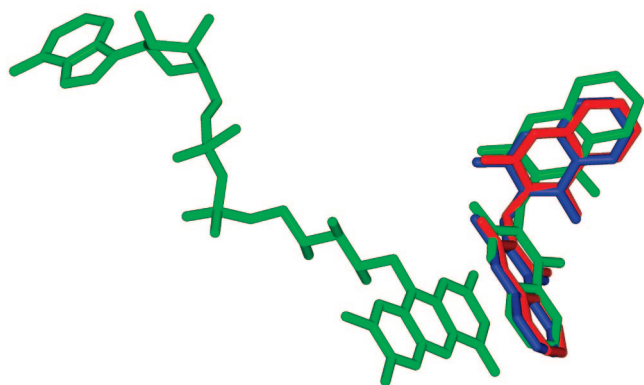


Figure 3. Dicoumarol and FAD from the docked dianionic (blue), docked monoanionic (red), and crystal (green) complexes.

dianion and monoanion poses of **2** have internal geometries reflected by $\varphi\psi$ linker torsion angles of (86° , -88°) and (80° , 80°), respectively. The docked monoanionic pose of **2** is therefore quite distinct from X-ray pose of **1**, which has $\varphi\psi$ values of (82° , -97°) and reflects a flipped conformation, where the relative orientation of the two coumarin rings have oxygens O2 and O2'' proximal with oxygens O4'' and O4, respectively (Figure 5B). Otherwise, there is overall similarity to **1** in terms of bent shape and π -stacking (Figure 5B); indeed, an alternative docked solution of **2**, 0.3 kcal/mol less favorable than the lowest energy, features the coumarin rings in the orientation observed crystallographically for **1**.

Molecular Dynamics Simulations. To obtain further detail on the conformation, dynamics and protonation state of **1** and **2** in the active sites of NQO1, we performed four molecular dynamics simulations of the NQO1 complexes in explicit solvent, each of six nanoseconds. Initial geometries of **1** and **2** in NQO1 were constructed using the NQO1/**1** crystal structure. Ligands were modeled in both active sites of NQO1 dimer. At the pH of crystallization (8.1),²⁰ an approximately equal proportion of monoanionic and dianionic species could potentially form. Therefore, simulations using either the monoanionic or dianionic form of **1** and **2** were conducted.

We first consider simulations of ligand **1** in complex with NQO1. We observe that when dicoumarol **1** is treated as the dianion, a conformational transition is observed in the relative intramolecular orientation of the two coumarin rings in the active site of NQO1. For one dicoumarol molecule, this occurs at 3.9 ns (Figure 6A), switching from an initial average $\varphi\psi$ value of (52° , -123°) to a final orientation of (118° , 125°). For the

dicoumarol in the other NQO1 active site, a transition is observed from (56° , -122°) to (125° , 122°) at 5.3 ns (Supporting Information Figure S1). These final conformations retain the overall bent shape of dicoumarol but, as witnessed for the docked structure of monoanionic **2** above, correspond to a flip in the relative orientation of the two coumarin rings (here by an angle of $\sim 120^\circ$ with respect to the plane of the coumarin rings) such that oxygens O2 and O2'' are now proximal with oxygens O4'' and O4, respectively. The transition to this structure is coupled to a distancing and tilting of the coumarin ring away from a FAD-stacked sandwich orientation (Supporting Information Figure S2), with an average inter-ring centroid distance of 5.5 ± 0.4 and 7.4 ± 4.6 Å between the terminal heterocyclic ring of FAD and the heterocyclic 6-membered ring of dicoumarol. This compares with a distance in the crystal structure of 3.6 Å. Particularly, the second of these two distinct dianionic conformations sampled during MD is somewhat different from that observed in the crystal structure, which has a $\varphi\psi$ value of (82° , -97°). The large error bar of 4.6 Å is indicative of an increasing distance.

By contrast, the monoanionic dicoumarol/NQO1 simulation maintained a single-ligand conformation in good agreement to that observed crystallographically (Figure 6A), with average linker torsion values of ($85 \pm 0^\circ$, $-114 \pm 1^\circ$) and ($88 \pm 3^\circ$, $-112 \pm 2^\circ$). This dicoumarol conformation appears to be stabilized by a persistent charge-assisted intramolecular H4...O4'' hydrogen bond, with average distances of 1.66 ± 0.01 and 1.69 ± 0.02 Å for the two molecules of **1** in the two active sites of NQO1 dimer. The average inter-ring centroid distances between FAD and dicoumarol here are 4.9 ± 0.1 and 4.6 ± 0.5 Å. The difference in intramolecular dicoumarol conformation as a function of its charge is also reflected by differing protein contacts. For the monoanion, the crystallographically observed dicoumarol O4...N ϵ_2 His161 hydrogen bond is 100 and 98% occupied by the two ligand molecules (Figure 7A), whereas for the dianion, this decreases to 25% for one ligand and is lost for the other. Similarly, in reasonable agreement with the protein–ligand contacts observed in the crystal structure, for the monoanion, the Tyr128 H η ...O2 dicoumarol hydrogen bond is 55 and 36% occupied, and a Tyr128 H η ...O1 interaction is 36 and 27% populated. For the dianion of **1**, these hydrogen bonds are not occupied, but instead, stronger interactions are made with His194 (a fairly flexible surface-exposed residue), with 48 and 30% occupancies for atom N ϵ_2 contacts with ligand oxygens O2 and O2''.

Corresponding MD simulations were performed on the NQO1 complex of **2**. Compound **2** was modeled in both monoanionic and dianionic forms using the crystallographic pose of dicoumarol. For simulation of the dianionic form of **2**, one ligand molecule displays considerable flexibility in the active site, oscillating mainly between two rotamers corresponding to $\pm 30^\circ$ with respect to an eclipsed relative orientation of the coumarin rings (Figure 6B). The motion appears to be linked to a similar distancing and tilting of the coumarin ring away from a FAD-stacked sandwich orientation, with an average inter-ring centroid distance of 5.2 ± 0.7 Å between the terminal heterocyclic ring of FAD and the heterocyclic 6-membered ring of dicoumarol.

No major conformational transition in ligand conformation was observed over six nanoseconds for simulation of monoanionic **2** in either active site of NQO1: the $\varphi\psi$ torsion angles in monoanionic **2** librated around averages value of ($89 \pm 3^\circ$, $-113 \pm 3^\circ$) and ($88 \pm 2^\circ$, $-116 \pm 4^\circ$) (Figure 6B), close to the (82° , -97°) minimum occupied by the crystal structure of **1**/NQO1. As with the simulation of dicoumarol, a strong intramolecular

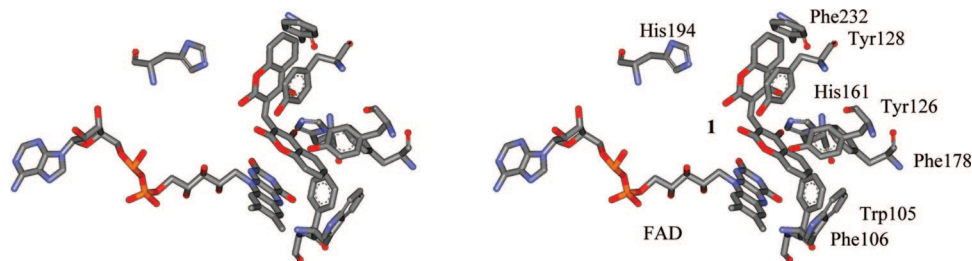


Figure 4. Stereoview of the crystallographic pose of dicoumarol **1** in the active site of hNQO1.

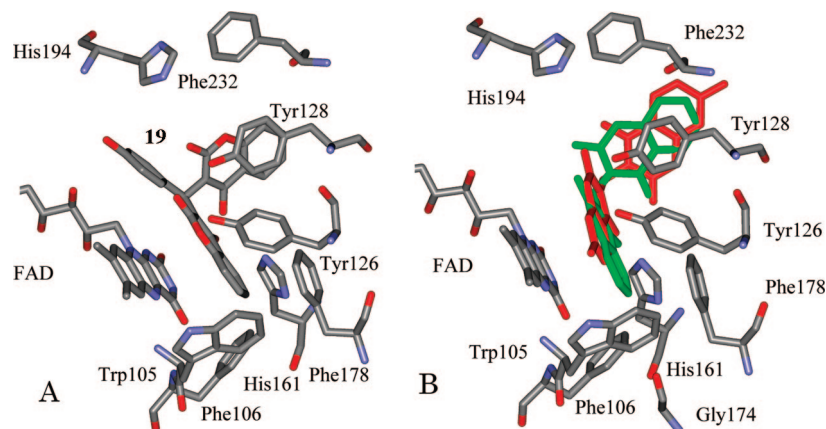


Figure 5. Docked pose in active site of NQO1 of (A) monoanionic **19** and (B) monoanionic **2** (red) superimposed on the crystal pose of **1** (green). Close polar contacts are indicated.

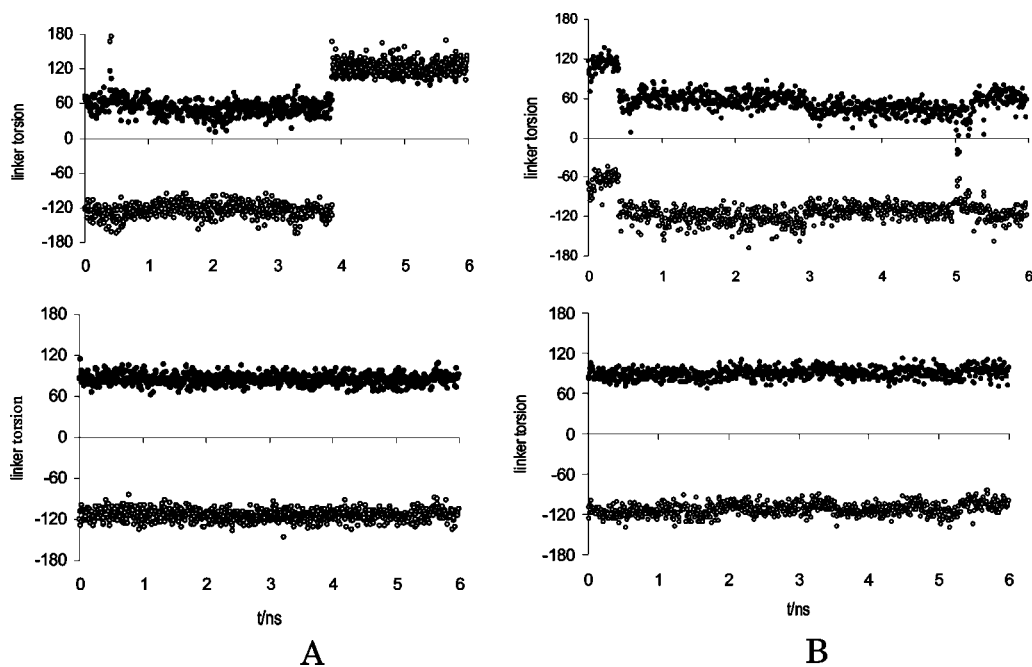


Figure 6. Time series for torsion angles φ (black circles) and ψ (white circles) of CH_2 linker in (A) dianionic **1** (top) and monoanionic **1** (bottom) and (B) dianionic **2** (top) and monoanionic **2** (bottom), from MD initiated from NQO1 crystal structure 2F1O. Angles are given in degrees.

hydrogen bond is found for each of the two ligands, with average $\text{H4}''\cdots\text{O4}$ distances of 1.66 ± 0.01 and 1.63 ± 0.02 Å. A similar pattern of protein–ligand interactions for dianionic and monoanionic forms of **2** is found to that of dianionic and monoanionic forms of dicoumarol: the same contacts to His161 and Tyr128 are populated for the monoanion (Figure 7A and B), whereas hydrogen bonds to His194 are observed for the dianion. We do note that interaction with His161 is maintained in the dianion for one of the ligands (occupancy of 100% for the His161

$\text{N}\epsilon_2\text{-H}\cdots\text{O4}$ hydrogen bond). In simulations of monoanionic **2**, one of the additional 7-hydroxy groups is directed toward the Trp105 ring, potentially providing additional electrostatic stabilization, with average dicoumarol $\text{H7}\cdots\text{Trp105}$ heterocycle centroid distances of 2.8 ± 0.2 and 2.5 ± 0.1 Å. The stability of this pose found in the MD may in part arise from this interaction and from the incorporation of active site flexibility, both of which were omitted during docking calculations.

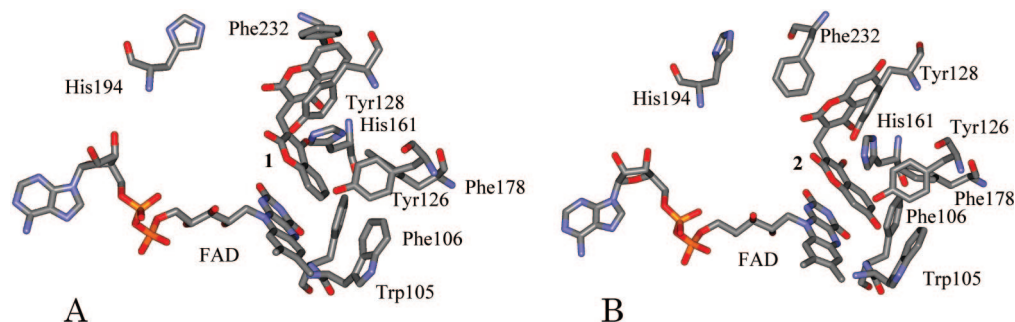


Figure 7. Representative structures from MD trajectory of (A) monoanionic dicoumarol **1** and (B) monoanionic **2** in active site of NQO1.

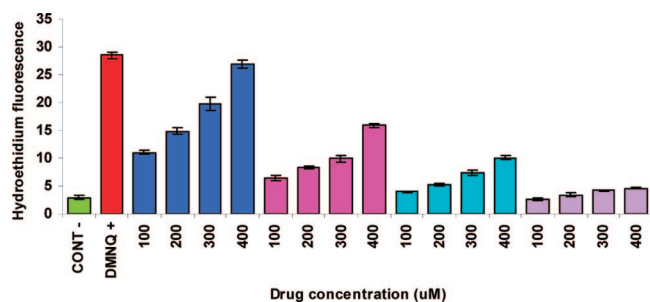


Figure 8. Superoxide generation in MIA PaCa-2 cells treated with various drug concentrations (0–400 μM). Cells received no treatment (green) and DMNQ was used as a positive control (red). Dicoumarol (**1**) treated cells (blue), **2** (pink), **23** (aqua), and **22** (purple). The cells were incubated with dihydroethidium (10 μM) and fluorescence quantitated by flow cytometry. Results shown are the mean \pm SD of three independent experiments.

Table 2. Effect of NQO1 Inhibitors on the Rate of Respiration in MIA PaCa-2 Cells

treatment	O ₂ consumption ^a
untreated	2.5 \pm 0.3
1 (100 μM)	7.0 \pm 0.4
2 (100 μM)	2.6 \pm 0.3
22 (100 μM)	2.5 \pm 0.4
23 (100 μM)	2.5 \pm 0.3

^a nmol O₂/min/10⁶ cells \pm SD; *n* = 3 independent determinations.

Effects on Pancreatic Tumor Cells. Here, we assess four of the NQO1 inhibitors considered above in terms of their ability to produce potentially unselective and undesirable effects in cells, namely, superoxide generation and alteration in oxygen consumption. These properties are evaluated in pancreatic cancer cells as modeled by the MIA PaCa-2 cell line. We also consider the ability of these compounds to kill MIA PaCa-2 cells and inhibit their growth. The four ligands are dicoumarol, **2**, **22**, and **23** (Table 1). In agreement with Lewis et al.,²³ we find that dicoumarol has the ability to generate superoxide (Figure 8). However, the three analogues show a substantially reduced capacity to do this (Figure 8).

Similarly, the rate of respiration increases in MIA PaCa-2 cells on addition of dicoumarol: 100 μM dicoumarol causes an immediate 3-fold increase in oxygen consumption, whereas the same concentration of each of the three analogues has no effect (Table 2).

Finally, we assess the pancreatic cell toxicity of dicoumarol and the three analogues, using MIA PaCa-2 cells. The cells were held in full growth medium (containing 10% fetal calf serum) and exposed to various concentrations of each compound for 96 h prior to MTT assay. The IC₅₀ cytotoxicity values for **1**, **2**, **22**, and **23** were determined to be 75, 190, 150, and 140 μM , respectively. To complement this, growth curves were estab-

lished for MIA PaCa-2 cells treated with the four compounds (Figure 9). All the compounds inhibit cell growth, demonstrating a comparable dose-dependent reduction in the doubling time when compared to that of the untreated control.

Discussion

We have identified new coumarin-based inhibitors of hNQO1, one of which displays equivalent potency to the strongest known competitive inhibitor of this enzyme, dicoumarol **1**. This ligand, **2**, differs from dicoumarol in possessing two 7-hydroxyl groups in each coumarin ring. Computational docking studies indicate these compounds bind in a similar overall conformation and active site location and highlight the importance of lipophilic interactions. MD simulations suggest differences in relative orientation of coumarin rings in the NQO1 complexes of **1** and **2** depending on charge state of dicoumarol, with evidence in the dianionic forms of conformational flexibility around the connecting linker moiety. This could be related to some uncertainty in the assigned ligand orientation in the dicoumarol/NQO1 crystal structure (resolution = 2.75 Å) and, in particular, the average atomic B-factor of the second coumarin ring (71.2 Å²). Potentially, both dianionic and monoanionic charge states of **1** and **2** could be present in the crystal at pH 8.1, although this depends on the local pK_a of the ligands in the active sites. The observed high affinity of **1** and **2** for NQO1, in light of apparent ligand disorder in the crystal structure, could therefore be caused by the presence of multiple tightly bound conformations (formed principally from good lipophilic contacts), which would have additional entropic benefit. However, our MD simulations indicate quite distinct protein contacts with NQO1 for dianionic versus monoanionic ligands, with the monoanionic forms making contacts in agreement with the crystal structure. No doubt this is, in part, a function of intramolecular interoxygen repulsion in **1** and **2**, with a resulting effect on ligand conformation (Figure 6) and protein–ligand contacts. Although the simulations of monoanionic **1** and **2** do agree well with the dicoumarol/NQO1 crystal structure, we note the exception of the CH₂ linker bond angle (C3–C1′–C3′′), where the value from the simulations of dianionic **1** and **2** (112–114°) was in better agreement with the crystal value (117.8°) than with monoanionic values (106–107°). However, given the overall better agreement of the monoanionic simulations with the **1**/NQO1 crystal structure in terms of ligand conformation and protein–ligand interactions, we suggest that monoanionic forms of **1** and **2** are the species present in the crystal structure and most probably the dominant forms under assay conditions. The high observed ligand B-factors may correspond to flexibility in the monoanionic ligands not sampled on the MD time scale here or to equilibria associated with various monoanionic tautomers.

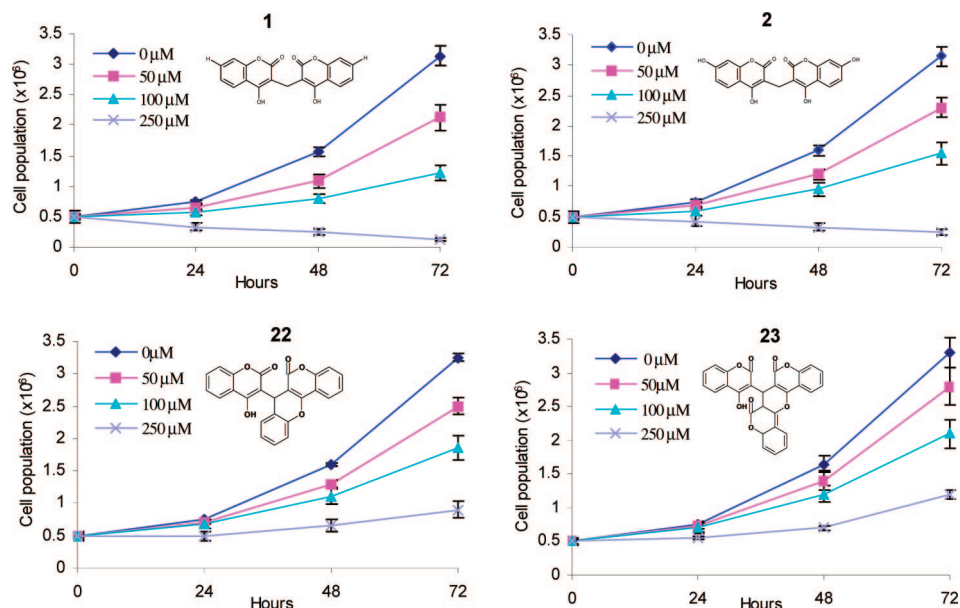


Figure 9. Growth curves for MIA PaCa-2 cells treated with dicoumarol **1**, **2**, **22**, and **23** (0, 50, 100, and 250 μM). Each point was determined in triplicate from the same culture; $n = 3$ independent experiments.

Cell-based studies indicate that three of these inhibitors (**2**, **22**, and **23**), of varying NQO1 inhibitory potency, display markedly less off-target effects compared to dicoumarol, with reduced effects on superoxide production and little impact on respiration rate. Interestingly, the compounds exhibit a similar ability to dicoumarol in terms of pancreatic tumor cell toxicity and growth inhibition. The observed properties of this set of coumarin-based inhibitors suggest a number of conclusions.

First, given that weaker NQO1 inhibitors **23** and **22** have similar effects on cell toxicity and growth as the more potent dicoumarol and **2** compounds, it appears the ability of dicoumarol to kill pancreatic cancer cells (as modeled by the MIA PaCa-2 cell line in which p53 is absent) is at least to some extent independent of NQO1 inhibition. This is in agreement with recent work using a series of indolequinone mechanism-based inhibitors of NQO1, where the growth inhibitory effect in pancreatic cancer cells did not correlate with extent of NQO1 inhibition.²⁴

Second, compared to dicoumarol, compound **2** has a much reduced effect on both cellular superoxide levels and oxygen consumption. It is interesting that this difference arises merely from the addition of two hydroxyl groups at the 7-position of each coumarin ring. Consequently, the increased superoxide production of dicoumarol may be linked to its ability to decouple mitochondrial respiration rather than inhibition of NQO1 in its role as a potential superoxide scavenger. Indeed, dicoumarol has been used as a mitochondrial uncoupling agent for many years, and it is known that uncoupling of mitochondrial function can lead to increased levels of intracellular superoxide. Furthermore, Ough et al.²⁵ have showed that production of superoxide and cytotoxicity induced by dicoumarol was significantly reduced following transfection of MIA PaCa-2 cells with manganese superoxide dismutase. Since manganese superoxide dismutase is predominantly located within mitochondria, it is possible that dicoumarol could be targeting mitochondria directly.

Third, we note that despite increased superoxide levels generated by dicoumarol and the range in NQO1 inhibitory potency exhibited by the four compounds, these molecules are similar in cytotoxicity and inhibition of pancreatic tumor cell

growth. The slightly greater toxicity of dicoumarol in MIA PaCa-2 cells relative to the other compounds may have its basis in mitochondrial uncoupling or superoxide generation, but this seems unlikely to be the underlying mechanism of cell growth inhibition. This conclusion is in line with recent work by Dehn et al.²⁶ who observed inhibition of pancreatic tumor cell growth using a mechanism-based NQO1 inhibitor, ES936, but did not observe an increase in intracellular superoxide production or oxygen consumption after treatment of cells with ES936. Our results further suggest that inhibition of NQO1 per se is unlikely to be the major underlying mechanism by which the compounds described here kill pancreatic cancer cells.

Conclusion

In this study, we have identified new coumarin-based inhibitors of NQO1 with varying potency. Structure–activity relationships for linker-substituted dicoumarol analogues indicate the effects of steric hindrance, as well as the importance of forging nonpolar interactions in the active site of NQO1. Compound **2** inhibits NQO1 to the same extent as dicoumarol. Differing from dicoumarol by two hydroxyl groups, computational docking studies indicate these compounds occupy a similar active site region. Molecular dynamics simulations of the dianionic and monoanionic forms of **1** and **2** in the NQO1 active sites were performed. The best agreement with the **1**/NQO1 crystal structure is found by treatment of **1** and **2** as the monoanion, suggesting these species are dominant under crystallization conditions and most probably under assay conditions.

Selected inhibitors were then assessed for off-target effects and were found to have different effects from dicoumarol regarding superoxide generation and oxygen respiration. Using these inhibitors as probes, we conclude that (1) the ability of dicoumarol to kill MIA PaCa-2 carcinoma cells is unlikely to depend upon NQO1 inhibition and that cytotoxicity may only be dependent on superoxide formation to a limited extent and (2) superoxide production does not seem to be linked to NQO1 inhibition but may be related to mitochondrial uncoupling. Therefore, within the limits of the MIA PaCa-2 cell model, this may suggest the existence of an alternative mechanism for the observed effect of dicoumarol on pancreatic tumors, possibly

mediated by its other known ancillary effects, which include inhibition of glutathione transferases and peroxidases and NADH-ubiquinone reductase. Finally, we note that these inhibitors may also prove to be useful as probes in the characterization of the involvement of NQO1 in cancer cells where tumor suppressor protein p53 is present.

Experimental Methods

Chemicals. Compounds **1** and **24** were commercially available (we note that **24** can be prepared as described in ref 27). Compounds **2–6**, **8–11**, **14–23**, **25**, and **26** (Table 1) were previously reported in ref 28. Compounds **7**, **12**, and **13** were obtained from the NCI repository (www.dtp.nci.nih.gov). Alternative labeling schemes used for compounds **2–26** are given in Table 1S (Supporting Information).

Molecular Modeling. For docking and molecular dynamics studies, coordinates for NQO1, a dimeric protein, were obtained from the crystal structure of the hNQO1/dicoumarol complex (PDB code 2F1O,²⁰ resolution = 2.75 Å). For preparation of ligand structures, dicoumarol analogue 2D structures were obtained from the NCI via a substructure search of the NCI database, based on the SMILES string of dicoumarol. 3D coordinates were assigned using CORINA.²⁹ Of the 54 analogues identified, 25 compounds were selected based on availability and were supplemented by one additional coumarin-based ligand, **24**. The pK_a values of dicoumarol have been experimentally determined to be 3.9 ± 0.2 and 8.0 ± 0.1.³⁰ Under assay (pH 7.4) and crystallization conditions (pH 8.1), a mixture of dianionic and monoanionic species would therefore be expected to exist. We consider both states in our docking and molecular dynamics studies here. For the monoanionic species, a number of tautomers are possible. Through quantum chemical calculations using the electronic-structure package Gaussian 03,³¹ we examined two possible tautomers of 4-hydroxycoumarin: protonation at the 2- and 4-positions (Supporting Information Figure S4). At the B3LYP/6-311++G(2d,2p) level of theory, the 4-H form was found to be 5–6 kcal/mol more favorable than the 2-H forms (Figure S4); therefore the form of **1** in which the 4-position was protonated on one of the rings was adopted for subsequent modeling studies (Figure 1B). Ligand **24** was constructed using SYBYL 6.8 (Tripos Ltd., St. Louis, MA). Ligands were subject to 1000 iterations of energy minimization using the steepest descent algorithm using the MMFF94 forcefield.³²

Docking. Flexible ligand docking to NQO1 was performed using the computer program GOLD 2.2.¹⁵ The NQO1 dimer was used for docking purposes, and the docking calculations were performed on one of the two identical active sites. Hydrogens atoms were added, and their positions were optimized using SYBYL. The active site of human NQO1 was defined on the basis of the ligand position in 2F1O, as amino acids with atoms falling within a 5 Å radius sphere of ligand atoms. GOLD uses a genetic algorithm (GA) whereby the molecular features of a protein–ligand complex are encoded as a chromosome. Each GA run comprised 100 000 genetic operations on an initial population of 100 members divided into five subpopulations. Operator weights for crossover, mutation, and migration were set to 95, 95, and 10, respectively. GOLD allows a user-definable number of GA runs per ligand, each of which starts from a different orientation. For these experiments, the number of GA runs was set to 10, and scoring of the docked poses was performed with the ChemScore scoring function.¹⁶ The top five solutions for each ligand were retained and analyzed for favorable interactions in the NQO1 active site including low protein–ligand clash and ligand distortion energies.

Molecular Dynamics. Initial structures for MD of the NQO1 complexes of ligands **1** and **2** were based on the X-ray geometry of hNQO1–dicoumarol.²⁰ Hydrogens atoms were added using the WHATIF³³ program to optimize hydrogen bond networks. Ligands were modeled in both of the symmetric active sites of NQO1 dimer. Nonstandard residues (FAD and ligands) were assigned AM1-BCC charges³⁴ and nonelectrostatic parameters from the generalized Amber force field.³⁵ The tautomeric states of histidine residues were

determined according to the local environment. Chloride anions were added to neutralize the system. Prior to minimization and MD, the enzyme–inhibitor complex was immersed in a box of TIP3P water. Periodic boundary conditions were imposed in conjunction with the particle-mesh Ewald method³⁶ for long-range electrostatics interactions. A cutoff of 8 Å was used for Lennard-Jones interactions, and SHAKE³⁷ was used to constrain bond lengths between heavy atoms and hydrogens. MD simulations using the AMBER suite of programs³⁸ were performed at 300 K with a time step of 2 fs. Energy minimization was followed by a short MD simulation, in combination with restraints, to remove unfavorable contacts of water and counterions and to fill vacuum pockets while keeping the initial conformation of the protein complex fixed. Subsequent equilibration involved smoothly decreasing harmonic restraints on the complex and alternating P and V constraints, completing with a 60 ps NVT simulation³⁹ without constraints. After a total equilibration of 200 ps, 6 ns of production dynamics was acquired in the NVT ensemble. As a measure of equilibration for the four compounds studied by molecular dynamics (vide infra), the root-mean-square deviation of protein backbone atoms was monitored, converging in each case to a value of around 2 Å (Supporting Information Figure S5). For analysis, ligand CH₂ linker torsion C2–C3–C1'–C3'' is denoted φ , and C3–C1'–C3''–C2'' is denoted ψ (Figure 1A). Hydrogen bond occupancy was calculated using a donor–acceptor heavy atom distance cutoff of 3.5 Å and a deviation from linearity in hydrogen bonding angle of up to 60°. Errors in MD averages were estimated using block averaging.

Inhibition of NQO1. Recombinant human NQO1 was prepared and purified as described by Phillips.⁴⁰ The enzyme was then diluted in 50 mM phosphate buffer to give an absorbance of 0.1 at 550 nm; 5 μ L of this solution was then mixed with 495 μ L of 50 mM phosphate buffer at pH 7.4 containing 200 μ M NADH, 70 μ M cytochrome *c*, 5 μ M menadione, with or without 2 μ M BSA, and various concentrations of the potential inhibitor dissolved in DMSO (final concentration 0.5% v/v). On some occasions, potential inhibitors were dissolved in 0.13 M NaOH. The concentration of menadione was chosen to correspond to the K_m value for this substrate determined under the same conditions. Reactions were carried out at 25 °C, and cytochrome *c* reduction was monitored at 550 nm in a Beckman DU 650 spectrophotometer. IC₅₀ values were determined using nonlinear curve fitting as implemented in the program Excel for which a 50% reduction of the initial rate was attained.

Detection of Intracellular Superoxide. Intracellular superoxide production was measured using the oxidation of dihydroethidium. For these experiments, exponentially growing human pancreatic MIA PaCa-2 cells were harvested by trypsinization, washed in PBS, counted using a hemocytometer, and 1 × 10⁶ cells were treated with vehicle (NaOH), the NQO1 inhibitors, or 50 μ M dimethylnaphthoquinone (DMNQ, as positive control) in complete media for 4 h at 37 °C. After drug treatment, 10 μ M dihydroethidium was added, and the cells were incubated for an additional 30 min. Subsequently, the cells were centrifuged and resuspended in 1 mL of PBS. Conversion of dihydroethidium to a fluorescent oxidized product was measured by flow cytometry (FACScan, Becton–Dickinson).

Measurement of Oxygen Respiration. MIA PaCa-2 cells were harvested by trypsinization, washed in PBS, counted, and resuspended in complete media at 37 °C. Oxygen consumption was measured in complete medium with 2 × 10⁶ cells in suspension at 37 °C. The oxygen utilization was measured over 15 min, and oxygen consumption was calculated over a 5 min time period. Calculations of dissolved oxygen were corrected for temperature (37 °C) and pressure (762 mmHg).

Cytotoxicity Assays. MIA PaCa-2 cells were exposed to varying concentrations of each compound for 96 h. The number of surviving cells was then determined by the use of the MTT assay.⁴¹ Values of IC₅₀ are the drug concentrations required to reduce cell number by 50% over this time period relative to untreated, control cells.

Acknowledgment. The authors gratefully acknowledge MRC Programme grant support (I.J.S.) and an MRC Chemical

Biology PhD studentship (K.A.N.). D.R. and D.S. were supported by HHS CA11441. We thank Natasha Wind and Edwin Chinje (funded via an EU Programme grant EUROXY project) for technical support with this study. This research was supported in part by the Intramural Research Program of the NIH, NCI. We thank Dr Phil Edwards for helpful discussions.

Supporting Information Available: Table of alternative labeling of compounds 2–26. time series for torsion angles φ and ψ of CH₂ linker in monoanionic and dianionic forms of 1 from MD initiated from the crystal structure, representative structures from MD trajectory of binding mode for dianionic 1 and 2, time series for torsion angles φ and ψ of CH₂ linker in monoanionic and dianionic forms of 2 from MD initiated from the crystal structure, structure and relative energies (kcal/mol) of tautomers of 4-hydroxycoumarin calculated at the B3LYP/6-311++G(2d,2p) level of theory, and backbone rmsd for the trajectories of tautomers of molecules 1 and 2 in complex with NQO1. This material is available free of charge via the Internet at <http://pubs.acs.org>.

References

- Ernster, L.; Navazio, F. Studies on TPN-linked oxidations. I. Pathways of isocitrate oxidation in rat liver mitochondria. *Biochim. Biophys. Acta* **1957**, *26*, 408–415.
- Jaiswal, A. K.; McBride, O. W.; Adesnik, M.; Nebert, D. W. Human dioxin-inducible cytosolic NAD(P)H: menadione oxidoreductase, cDNA sequence and localisation of gene to chromosome 16. *J. Biol. Chem.* **1988**, *263*, 13572–13578.
- Ernster, L. DT-diaphorase. *Method. Enzymol.* **1967**, *10*, 309–317.
- Li, R.; Bianchet, M. A.; Talay, P.; Amzel, L. M. The three-dimensional structure of NAD(P)H:quinone oxidoreductase, a flavoprotein involved in cancer chemoprotection and chemotherapy: Mechanism of the two-electron reduction. *Proc. Natl. Acad. Sci. U.S.A.* **1995**, *92*, 8846–8850.
- Ernster, L.; Ljunggren, M.; Danielson, L. Purification and some properties of the highly dicoumarol-sensitive liver diaphorase. *Biochem. Biophys. Res. Commun.* **1960**, *2*, 88–92.
- Seigel, D.; Bolton, E. M.; Burr, J. A.; Liebler, D. C.; Ross, D. The reduction of α -tocopherolquinone by human NAD(P)H: quinone oxidoreductase: The role of α -tocopherolquinone as a cellular antioxidant. *Mol. Pharmacol.* **1997**, *52*, 300–305.
- Gaikwad, A.; Long, D. J.; Stringer, J. L.; Jaiswal, A. K. In vivo role of NAD(P)H:quinone oxidoreductase 1 (NQO1) in the regulation of intracellular redox state and accumulation of abdominal adipose tissue. *J. Biol. Chem.* **2001**, *276*, 22559–22564.
- Lewis, A.; Du, J.; Liu, J.; Ritchie, J. M.; Oberley, L. W.; Cullen, J. J. Metastatic progression of pancreatic cancer: Changes in antioxidant enzymes and cell growth. *Clin. Exp. Metastasis* **2005**, *22*, 523–32.
- Ross, D.; Kepa, J. K.; Winski, S. L.; Beall, H. D.; Anwar, A.; Seigel, D. NAD(P)H: quinone oxidoreductase 1 (NQO1): Chemoprotection, bioactivation, gene regulation and genetic polymorphisms. *Chem.–Biol. Interact.* **2000**, *129*, 77–97.
- Asher, G.; Bercovich, Z.; Tsvetkov, P.; Shaul, Y.; Kahana, C. 20S proteasomal degradation of onithine decarboxylase is regulated by NQO1. *Mol. Cell* **2005**, *17*, 645–655.
- Faig, M.; Bianchet, M. A.; Winski, S.; Hargreaves, R.; Moody, C. J.; Hudnott, A. R.; Ross, D.; Amzel, L. M. Structure-based development of anticancer drugs: complexes of NAD(P)H oxidoreductase 1 with chemotherapeutic quinones. *Structure* **2001**, *9*, 659–667.
- Tsvetkov, P.; Asher, G.; Reiss, V.; Shaul, Y.; Sachs, L.; Lotem, J. Inhibition of NAD(P)H:quinone oxidoreductase 1 activity and induction of p53 degradation by the natural phenolic compound curcumin. *Proc. Natl. Acad. Sci. U.S.A.* **2005**, *102*, 5535–5540.
- Bello, R. L.; Gomez-Diaz, C.; Navas, P.; Villalba, J. M. NAD(P)H: Quinone oxidoreductase 1 expression, hydrogen peroxide levels, and growth phase in hela cells. *Method. Enzymol.* **2004**, *382*, 234–243.
- Garten, S.; Wosilait, W. D. Comparative study of the binding of coumarin anticoagulants and serum albumins. *Biochem. Pharmacol.* **1971**, *20*, 1661–1668.
- Jones, G.; Willett, P.; Glen, R. C.; Leach, A. R.; Taylor, R. Development and validation of a genetic algorithm to flexible docking. *J. Mol. Biol.* **1997**, *267*, 727–748.
- Verdonk, M. L.; Cole, J. C.; Hartshorn, M. J.; Murray, C. W.; Taylor, R. D. Improved protein–ligand docking using GOLD. *Proteins* **2003**, *52*, 609–623.
- Kontoyianni, M.; McClellan, L. M.; Sokol, G. S. Evaluation of docking performance: Comparative data on docking algorithms. *J. Med. Chem.* **2004**, *47*, 558–565.
- Ferrara, P.; Gohlke, H.; Price, D. J.; Klebe, G.; Brookes, C. L. Assessing scoring functions for protein–ligand interactions. *J. Med. Chem.* **2004**, *47*, 3032–3047.
- Nolan, K. A.; Timson, D. J.; Stratford, I. J.; Bryce, R. A. In silico identification and biochemical characterisation of novel inhibitors of NQO1. *Bioorg. Med. Chem. Lett.* **2006**, *16*, 6246–6254.
- Asher, G.; Dym, O.; Tsvetkov, P.; Adler, J.; Shaul, Y. The crystal structure of NAD(P)H Quinone Oxidoreductase 1 in complex with the potent inhibitor dicoumarol. *Biochemistry* **2006**, *45*, 6372–6378.
- Cheng, Y.; Prusoff, W. H. The relationship between inhibition constant K_i and the concentration of inhibitor which causes 50% inhibition I_{50} of an enzymatic reaction. *Biochem. Pharmacol.* **1973**, *22*, 3099–3108.
- Winski, S. L.; Faig, M.; Bianchet, M. A.; Seigel, D.; Swann, E.; Fung, K.; Duncan, M. W.; Moody, C. J.; Amzel, M.; Ross, D. Characterization of a mechanism-based Inhibitor of NAD(P)H:Quinone Oxidoreductase 1 by biochemical, X-ray crystallographic, and mass spectrometric approaches. *Biochemistry* **2001**, *40*, 15135–15142.
- Lewis, A.; Ough, M.; Ling, L.; Hinkhouse, M. M.; Ritchie, J. M.; Spitz, D. R.; Cullen, J. J. Treatment of pancreatic cancer cells with dicoumarol induces cytotoxicity and oxidative stress. *Clin. Cancer Res.* **2004**, *10*, 4550–4558.
- Reigan, P.; Colucci, M. A.; Siegel, D.; Chilloux, A.; Moody, C. J.; Ross, D. Development of indolequinone mechanism-based inhibitors of NAD(P)H:quinone oxidoreductase 1 (NQO1), NQO1 inhibition and growth inhibitory activity in human pancreatic MIA PaCa-2 cancer cells. *Biochemistry* **2007**, *46*, 5941–5950.
- Ough, M.; Lewis, A.; Bey, E. A.; Gao, J.; Ritchie, J. M.; Bornmann, W.; Boothman, D. A.; Oberley, L. W.; Cullen, J. J. Efficacy of β -lapachone in pancreatic cancer treatment: Exploiting the novel, therapeutic target NQO1. *Cancer Biol. Ther.* **2005**, *4*, 95–102.
- Dehn, D. L.; Siegel, D.; Zafar, K. S.; Reigan, P.; Swann, E.; Moody, C. J.; Ross, D. 5-Methoxy-1,2-dimethyl-3-[(4-nitrophenoxy)methyl]-indole-4,7-dione, a mechanism-based inhibitor of NAD(P)H:quinone oxidoreductase 1, exhibits activity against human pancreatic cancer in vitro and in vivo. *Mol. Cancer Ther.* **2006**, *5*, 1702–1709.
- Ivanov, I.; Karagiozov, S.; Manolov, I. Synthesis of 4-(monoalkylamino)coumarins. *Arch. Pharm.* **1991**, *324*, 61–62.
- Zhao, H.; Neamati, N.; Hong, H.; Mazumder, A.; Wang, S.; Sunder, S.; Milne, G. W. A.; Pommier, Y.; Burke, T. R., Jr. Coumarin-based inhibitors of HIV integrase. *J. Med. Chem.* **1997**, *40*, 242–249.
- Gasteiger, J.; Rudolf, C.; Sadowski, I. Automatic generation of 3D-atomic coordinates for organic molecules. *Tetrahedron* **1990**, *3*, 537–547.
- Labbe-Bois, R.; Laruelle, C.; Godfroid, J. Quantitative structure–activity relationships for dicoumarol antivitamins K in the uncoupling of mitochondrial oxidative phosphorylation. *J. Med. Chem.* **1975**, *18*, 85–90.
- Frisch, M. J.; Trucks, G. W.; Schlegel, H. B.; Scuseria, G. E.; Robb, M. A.; Cheeseman, J. R.; Montgomery, J. A., Jr.; Vreven, T.; Kudin, K. N.; Burant, J. C.; Millam, J. M.; Iyengar, S. S.; Tomasi, J.; Barone, V.; Mennucci, B.; Cossi, M.; Scalmani, G.; Rega, N.; Petersson, G. A.; Nakatsuji, H.; Hada, M.; Ehara, M.; Toyota, K.; Fukuda, R.; Hasegawa, J.; Ishida, M.; Nakajima, T.; Honda, Y.; Kitao, O.; Nakai, H.; Klene, M.; Li, X.; Knox, J. E.; Hratchian, H. P.; Cross, J. B.; Bakken, V.; Adamo, C.; Jaramillo, J.; Gomperts, R.; Stratmann, R. E.; Yazyev, O.; Austin, A. J.; Cammi, R.; Pomelli, C.; Ochterski, J. W.; Ayala, P. Y.; Morokuma, K.; Voth, G. A.; Salvador, P.; Dannenberg, J. J.; Zakrzewski, V. G.; Dapprich, S.; Daniels, A. D.; Strain, M. C.; Farkas, O.; Malick, D. K.; Rabuck, A. D.; Raghavachari, K.; Foresman, J. B.; Ortiz, J. V.; Cui, Q.; Baboul, A. G.; Clifford, S.; Cioslowski, J.; Stefanov, B. B.; Liu, G.; Liashenko, A.; Piskorz, P.; Komaromi, I.; Martin, R. L.; Fox, D. J.; Keith, T.; Al-Laham, M. A.; Peng, C. Y.; Nanayakkara, A.; Challacombe, M.; Gill, P. M. W.; Johnson, B.; Chen, W.; Wong, M. W.; Gonzalez, C.; and Pople, J. A. *Gaussian 03*; Gaussian, Inc., Wallingford, CT, 2004.
- Clark, M.; Cramer III, R. D.; Van Opdenbosch, N. Validation of the general purpose MMFF94 5.2 force field. *J. Comput. Chem.* **1989**, *10*, 982–1012.
- Vriend, G. WHATIF: A molecular modelling and drug design program. *J. Mol. Graph. Model.* **1990**, *8*, 52–56.
- Jackalian, A.; Bush, B. L.; Jack, D. B.; Bayly, C. L. Fast, efficient generation of high-quality atomic charges. AM1-BCC model: I. Method. *J. Comput. Chem.* **2000**, *21*, 132–146.
- Wang, J. M.; Wolf, R. M.; Caldwell, J. W.; Kollman, P. A.; Case, D. A. Development and testing of a general Amber force field. *J. Comput. Chem.* **2004**, *25*, 1157–1174.
- Darden, T.; York, D.; Pedersen, L. Particle mesh Ewald: An N-log(N) method for Ewald sums in large systems. *J. Med. Chem.* **1993**, *98*, 10089–10092.

- (37) Van Gunsteren, W. F.; Berendsen, H. J. C. Algorithms for macromolecular dynamics and constraint dynamics. *Mol. Phys.* **1977**, *34*, 1311–1327.
- (38) Case, D. A.; Cheatham, III, T.E.; Darden, T. A.; Gohlke, H.; Luo, R.; Merz, K. M., Jr.; Onufriev, A.; Simmerling, C.; Wang, B.; Woods, R. J. The Amber biomolecular simulation programs. *J. Comput. Chem.* **2005**, *26*, 1668–1688.
- (39) Berendsen, H. J. C.; Postma, J. P. M.; van Gunsteren, W. F.; DiNola, A.; Haak, J. R. Molecular dynamics with coupling to an external bath. *J. Chem. Phys.* **1984**, *81*, 3684–3690.
- (40) Phillips, R. M. Bioreductive activation of a series of analogues of 5-aziridiny-3-hydroxymethyl-1-methyl-2-[1H-indole-4,7-dione] prop-beta-en-alpha-ol (EO9) by human DT-diaphorase. *Biochem. Pharmacol.* **1996**, *52*, 1711–1718.
- (41) Stratford, I. J.; Stephens, M. A. The differential hypoxic cytotoxicity of bioreductive agents determined in vitro by the MTT assay. *Int. J. Radiat. Oncol.* **1989**, *16*, 973–976.

JM070472P